



OPEN

Magnetic nano-sized solid acid catalyst bearing sulfonic acid groups for biodiesel synthesis and oxidation of sulfides

Durgesh Singh¹✉, Kamini Singh², Yashwantsinh Jadeja³, Soumya V. Menon⁴, Priyanka Singh⁵, Safaa Mohammed Ibrahim⁶, Manmeet Singh⁷, Munther Kadhim Abosaoda^{8,9}, Salwa Bader Al Reshaidan¹⁰ & Mohammed A. El-Meligy^{11,12}

In this study, the $\text{AlFe}_2\text{O}_4@n\text{-Pr}@Et\text{-SO}_3\text{H}$ heterogeneous catalyst was successfully synthesized and utilized to produce biodiesel from oleic acid through an esterification process and to oxidize sulfides. To examine the physicochemical characteristics of the $\text{AlFe}_2\text{O}_4@n\text{-Pr}@Et\text{-SO}_3\text{H}$ nanomaterial, a variety of advanced techniques were employed, including Fourier Transform infrared spectroscopy (FT-IR), Field emission scanning electron microscopy (FE-SEM), Energy dispersive X-ray spectroscopy (EDX), Vibrating sample magnetometer (VSM), Elemental Mapping, Transmission electron microscopy (TEM), Inductively coupled plasma (ICP), and X-ray diffraction (XRD). The $\text{AlFe}_2\text{O}_4@n\text{-Pr}@Et\text{-SO}_3\text{H}$ materials demonstrated excellent performance in both the esterification of oleic acid and the oxidation of sulfides. Moreover, the catalyst can be easily recovered and reused multiple times without a significant reduction in its effectiveness.

Keywords AlFe_2O_4 , Oleic acid, SO_3H , Sulfide

One of the important challenges in the synthesis of modern organic compounds is the development of efficient and new nanocatalysts^{1,2}. In recent times, there has been a growing interest in magnetic nanoparticles within the nanomaterial supports category³. This is because of their remarkable properties, including simple preparation and functionalization, a large surface area ratio, low toxicity, and cost-effectiveness⁴. The primary benefit of magnetic nanoparticles is the effortless separation of magnetic nanoparticles (MNPs) supported catalysts from a reaction product or mixture using an external magnet⁵⁻⁷. Based on these intriguing benefits, magnetic nanoparticles present a promising alternative to other catalyst supports, such as porous or mesoporous ones⁸. Recently, nanoscale compounds have garnered significant attention from researchers due to their unique chemical properties and catalytic applications⁹. These nanomaterials can serve as valuable supports for immobilizing homogeneous catalysts, effectively combining the benefits of both homogeneous and heterogeneous catalysis. Facilitating easy and rapid separation of catalysts from the reaction mixture is crucial in catalytic processes¹⁰. Traditionally, heterogeneous catalysts are recycled through tedious filtration processes, often resulting in the unavoidable loss of solid material. To address this, magnetic nanoparticles have been developed as suitable alternatives for catalytic reactions¹¹. In recent years, these nanoparticles have been extensively studied, as using an external magnet to separate the catalyst makes recovering catalysts from the reaction mixture much more convenient compared to traditional methods¹². AlFe_2O_4 nanoparticles have been extensively researched

¹Department of Chemistry, School of Chemical Sciences and Technology, Dr. Harisingh Gour Vishwavidyalaya (A Central University), Sagar 470003, India. ²Department of Chemistry, Deen Dayal Upadhyay Gorakhpur University, Gorakhpur 273009, India. ³Marwadi University Research Center, Department of Chemistry, Faculty of Science Marwadi University, Rajkot, Gujarat 360003, India. ⁴Department of Chemistry and Biochemistry, School of Sciences JAIN (Deemed to Be University), Bangalore, Karnataka, India. ⁵NIMS School of Allied Sciences and Technology, NIMS University Rajasthan, Jaipur 303121, India. ⁶Department of Optics Techniques, Health and Medical Techniques College, Alnoor University, Mosul, Iraq. ⁷Department of Applied Sciences, Chandigarh Engineering College, Chandigarh Group of Colleges-Jhanjeri, Mohali 140307, Punjab, India. ⁸College of Pharmacy, the Islamic University, Najaf, Iraq. ⁹College of Pharmacy, the Islamic University of Al Diwaniyah, Al Diwaniyah, Iraq. ¹⁰Department of Chemistry, Faculty of Science, King Saud University, P.O. Box 800, Riyadh 11451, Saudi Arabia. ¹¹Jadara University Research Center, Jadara University, PO Box 733, Irbid, Jordan. ¹²Applied Science Research Center, Applied Science Private University, Amman, Jordan. ✉email: durgesh.phdchem16@gmail.com

for their scientific significance and practical applications as a core magnetic support among various magnetic nanoparticles^{13,14}. The catalysis of chemical reactions by acids represents a consistently essential and captivating focus of research in organic synthesis^{15,16}. The development and application of robust solid acids as catalysts in synthetic reactions are promising for the future of organic synthesis, especially within the context of green chemistry^{17–19}. Immobilizing acidic functional groups on magnetic nanoparticles and utilizing them as catalysts in organic reactions is an ideal and fascinating solution to overcome this drawback^{20–22}. This is because the catalyst can be easily separated from the reaction media using an external magnet^{23,24}. Due to the rising energy consumption and the impending depletion of non-renewable fossil fuels, biodiesel has emerged as a promising alternative in the industrial sector^{25,26}. Biodiesel is a renewable, stable, sulfur-free fuel composed of monoalkyl esters of fatty acids, produced mainly by esterification of fatty acids with short-chain primary alcohols using acid–base catalysts^{26,27}. It is important to first esterify free fatty acids like oleic acid, linoleic acid, and others in incompatible feedstocks before using base catalysts for the transesterification reaction, as this helps prevent soap formation²⁸. Therefore, acid catalysis is more suitable for biodiesel production²⁹. In this case, the esterification reaction with a highly effective acid catalyst, without the need for any substrate pretreatment, can result in the production of eco-friendly biodiesel from oleic acid^{30,31}.

Organic sulfoxides serve as valuable synthetic intermediates in laboratories, industries, pharmaceuticals, and agrochemicals. The common method for synthesizing these materials involves the oxidation of sulfides³². Additionally, disulfides are crucial in various biological and chemical processes, including their use in sensor development, oil-sweetening procedures, vulcanizing agents, and more³³.

This work describes the synthesis and structural analysis of an innovative green catalyst. We also examine its effectiveness as an efficient and environmentally friendly option for Biodiesel Production. This solid acid catalyst showed effective catalytic performance in comparison to other solid acid catalysts previously reported (Fig. 1).

Experimental

Materials and Instrumentation The chemicals employed in this study were procured from Fisher and Merck. All reagents and solvents utilized throughout the research were acquired from Sigma-Aldrich, Fluka, or Merck and were used as received without any additional purification.

Preparation of $\text{AlFe}_2\text{O}_4@n\text{-Pr}@\text{Et-SO}_3\text{H}$

Magnetic nanoparticles (FeAl_2O_4) were prepared by the coprecipitation method. In a mixture of 80 mL ethanol and water (ratio 1:1) under a N_2 atmosphere at 80 °C, $\text{FeCl}_2 \cdot 4\text{H}_2\text{O}$ (10 mmol) and $\text{AlCl}_3 \cdot 9\text{H}_2\text{O}$ (20 mmol) were added. Then sodium hydroxide was added under stirring to obtain uniform black FeAl_2O_4 MNP nanoparticles. Once cooled, the samples were gathered using a permanent magnet and then meticulously washed several times with deionized water and EtOH. Subsequently, they were dried in a vacuum oven at 50 °C for 15 h.

To functionalize, 3-chloropropyltrimethoxysilane (n-Pr) (2.5 mL) was carefully added to a mixture of 1 g FeAl_2O_4 in 50 mL toluene. The resulting solution was stirred under nitrogen at 60 °C for 15 h to complete the

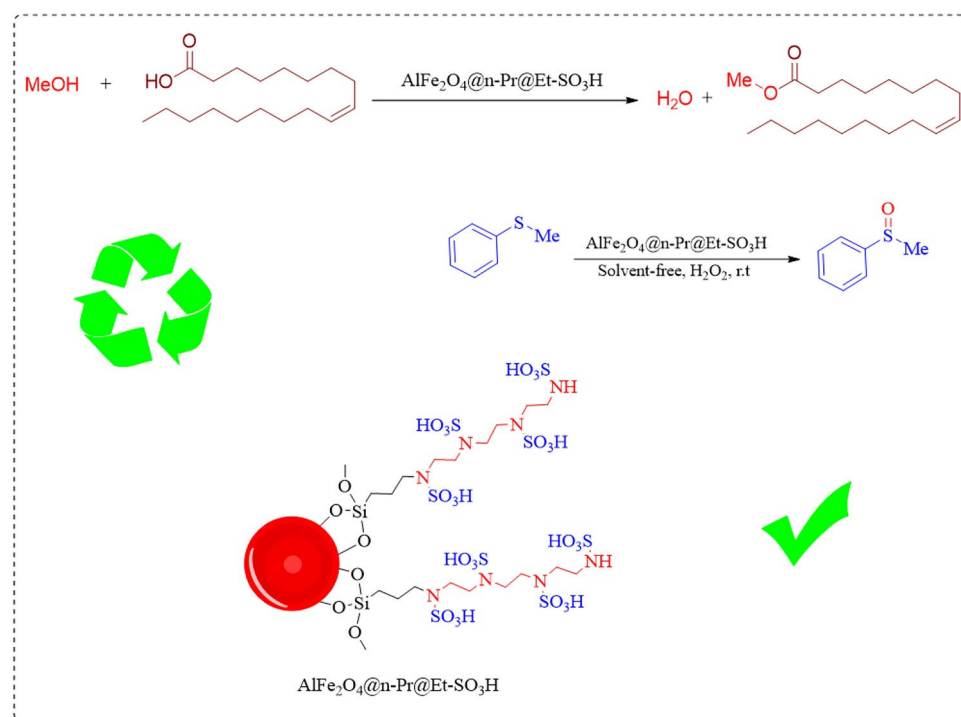
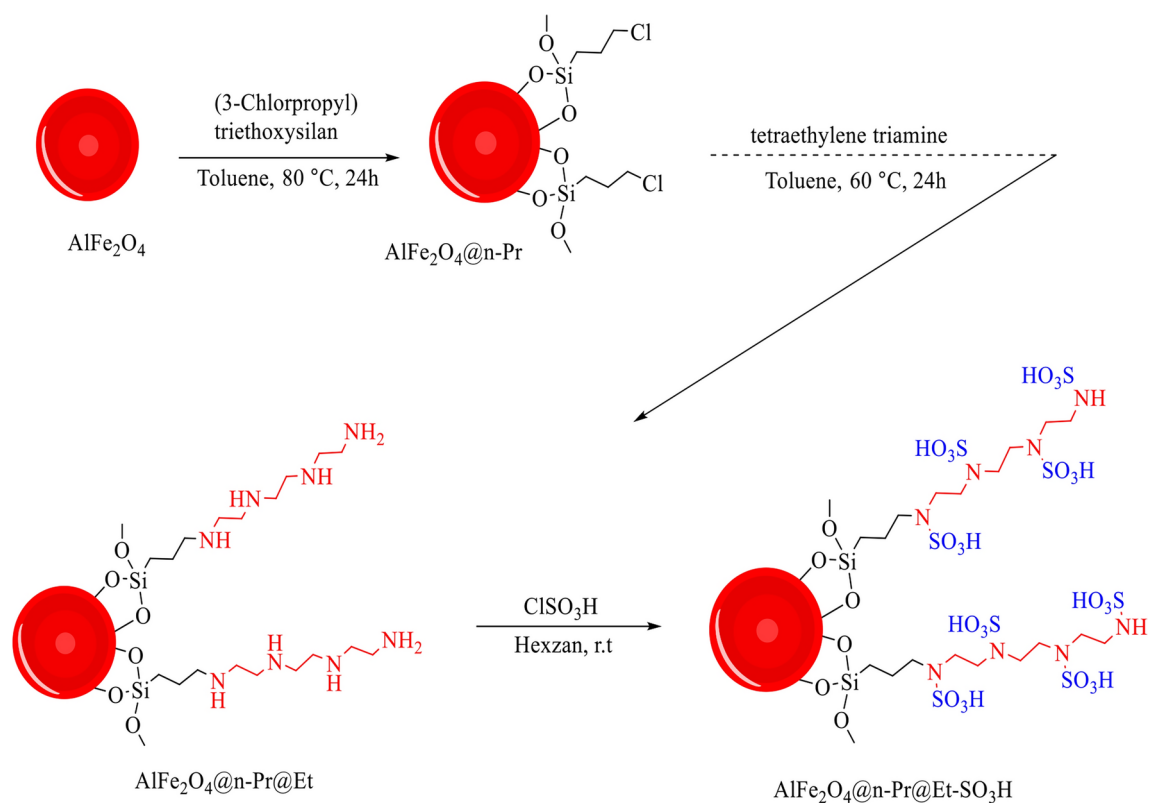
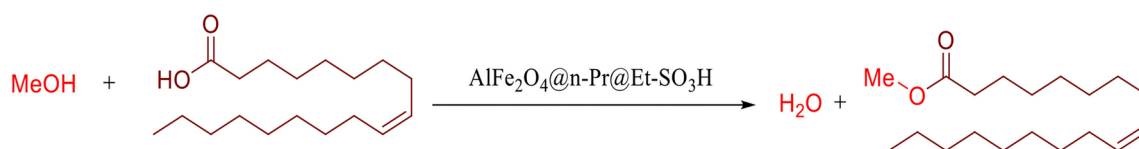


Fig. 1. Graphic abstract.



Scheme 1. Synthesis of $\text{AlFe}_2\text{O}_4@n\text{-Pr@Et-SO}_3\text{H}$.



Scheme 2. esterification of oleic acid.

process. After silanization, the solid material was separated using a magnet and thoroughly dried before being utilized in the subsequent process.

To prepare $\text{AlFe}_2\text{O}_4@n\text{-Pr@Et}$, 1 g of $\text{AlFe}_2\text{O}_4@n\text{-Pr}$ samples was dispersed in 20 mL of toluene. Then, 2.5 mmol of Triethylenetetramine (Et) was added to the reaction mixture, which was refluxed for 24 h. The $\text{AlFe}_2\text{O}_4@n\text{-Pr@Et}$ were then isolated using a magnet, washed with EtOH, and dried.

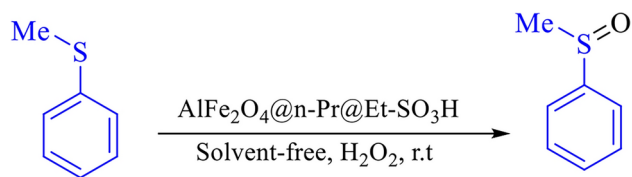
Finally, to prepare the $\text{AlFe}_2\text{O}_4@n\text{-Pr@Et-SO}_3\text{H}$ catalyst, a mixture of $\text{AlFe}_2\text{O}_4@n\text{-Pr@Et}$ (1.0 g) was dispersed in 80 ml of hexane in a round-bottomed flask. Next, 0.4 g of chlorosulfonic acid were carefully added drop by drop into the reaction vessel, and then the mixture was stirred at 25 °C for 24 h. Following the reaction, the resulting catalyst ($\text{AlFe}_2\text{O}_4@n\text{-Pr@Et-SO}_3\text{H}$) was subsequently isolated, purified with water and ethanol, and ultimately dried under vacuum at 55 °C (Scheme 1).

Biodiesel production

Initially, 3 mmol of oil, 12 mmol of methanol, and 0.04 g of catalyst were combined in a round bottom flask. After that, the blend was warmed to 60 °C and left for 2 h. Once the reaction was complete, the catalyst was filtered using a centrifuge, followed by the removal of excess methanol from the upper liquid phase using rotary evaporation. The organic phase that was extracted underwent an additional wash with distilled water to eliminate any remaining impurities and was then dried with anhydrous sodium sulfate (Scheme 2)^{34,35}.

A general procedure for the oxidation of sulfides

A combination of sulfide (1 mmol) and H_2O_2 33% (0.4 mL) was poured into the round-bottomed flask containing $\text{AlFe}_2\text{O}_4@n\text{-Pr@Et-SO}_3\text{H}$ (0.02 g). The resulting mixture was stirred at 25 °C without the use of any solvent. After the reaction was completed, the $\text{AlFe}_2\text{O}_4@n\text{-Pr@Et-SO}_3\text{H}$ compound was isolated using a magnet, and the resulting products were then extracted with a mixture of water and ethyl acetate. Subsequently, the organic



Scheme 3. Oxidation of sulfides catalyzed by $\text{AlFe}_2\text{O}_4@n\text{-Pr@Et-SO}_3\text{H}$.

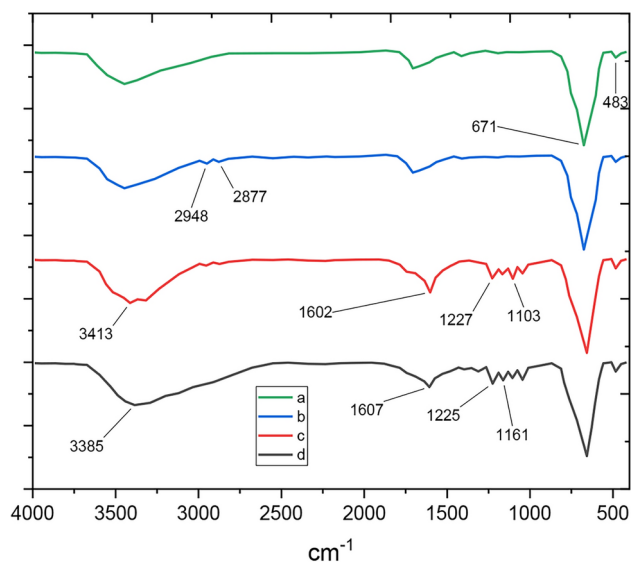


Fig. 2. FTIR spectra of (a) AlFe_2O_4 , (b) $\text{AlFe}_2\text{O}_4@n\text{-Pr}$, (c) $\text{AlFe}_2\text{O}_4@n\text{-Pr@Et}$, (d) $\text{AlFe}_2\text{O}_4@n\text{-Pr@Et-SO}_3\text{H}$.

substance mixture was dried using 1.5 g of anhydrous sodium sulfate. The solvent was then evaporated to obtain a high yield of pure sulfoxides (Scheme 3).

Selected NMR data

Methyl oleate: ^1H NMR (DMSO, 400 MHz) δ = 0.86 (s, 3H), 1.25 (s, 20H), 1.52 (m, 2H), 1.99 (s, 4H), 2.26 (s, 2H), 3.58 (s, 3H), 5.34 (d, 2H) ppm.

(Sulfinylbis(methylene))dibenzene: ^1H NMR (400 MHz, DMSO): δ_{H} = 7.4–7.5 (m, 10H), 4.36 (s, 4H) ppm.

(Ethylsulfinyl)ethane: ^1H NMR (400 MHz, DMSO): δ_{H} = 2.1 (q, 4H), 1.0 (t, 6H) ppm.

(Methylsulfinyl)benzene: ^1H NMR (400 MHz, DMSO): δ_{H} = 2.1 (q, 5H), 1.2 (t, 3H) ppm.

Results and discussion

After the $\text{AlFe}_2\text{O}_4@n\text{-Pr@Et-SO}_3\text{H}$ synthesis, EDX, TEM, VSM, FTIR, SEM, TGA, and XRD were employed to identify its nanostructure and nature accurately.

Catalyst characterizations

FT-IR spectra of AlFe_2O_4 (a), $\text{AlFe}_2\text{O}_4@n\text{-Pr}$ (b), and $\text{AlFe}_2\text{O}_4@n\text{-Pr@Et}$ (c) catalyst is shown in Fig. 2. The FT-IR spectrum of the AlFe_2O_4 NPs shows a stretching vibration at 3440 cm^{-1} , indicating the presence of both symmetrical and asymmetrical modes of the O–H bonds attached to the surface iron atoms (Fig. 2a). The FT-IR spectrum of AlFe_2O_4 nanoparticles exhibits two bands at 483 and 671 cm^{-1} , attributed to the stretching vibrations of the aluminum-oxygen and iron-oxygen bonds, respectively. In Fig. 2b, The appearance of new peaks at 2877 and 2948 cm^{-1} , which correspond to CH_2 bending vibration, respectively, provide evidence for modifying the surface of AlFe_2O_4 nanoparticles with 3-chloromethoxypropylsilane ($\text{AlFe}_2\text{O}_4@n\text{-Pr}$, Fig. 2c). In Fig. 2c, the existence of peaks at 1103, 1127, and 1602 cm^{-1} in Fig. 2c, which are allocated to C–N and N–H stretching absorptions of triethylenetetramine (Et), are indicative peaks for confirmation of $\text{AlFe}_2\text{O}_4@n\text{-Pr@Et}$ nanoparticles. The FT-IR spectrum in Fig. 2d confirmed the functionalization of $-\text{SO}_3\text{H}$ groups on $\text{AlFe}_2\text{O}_4@n\text{-Pr}$ through the absorption of OH stretching bands of the $-\text{SO}_3\text{H}$ moiety at $2500\text{--}3500\text{ cm}^{-1}$.

Figure 3 illustrates the normal angle powder X-ray diffraction (XRD) patterns for AlFe_2O_4 (a) and $\text{AlFe}_2\text{O}_4@n\text{-Pr@Et-SO}_3\text{H}$ (b). The XRD pattern of $\text{AlFe}_2\text{O}_4@n\text{-Pr@Et-SO}_3\text{H}$ closely resembles that of MFe_2O_4 , indicating the presence of octahedral structures. These patterns display a crystallized structure corresponding to the (2 2 0), (3 1 1), (2 2 2), (4 0 0), (4 2 2), (5 1 1), and (4 4 0) crystallographic faces of magnetite. The XRD results for AlFe_2O_4 confirm a crystalline cubic spinel structure characteristic of AlFe_2O_4 , aligning with standard reference data (JCPDS file, PDF no. 96–901-2447). After the attachment of sulfuric acid, a noticeable reduction

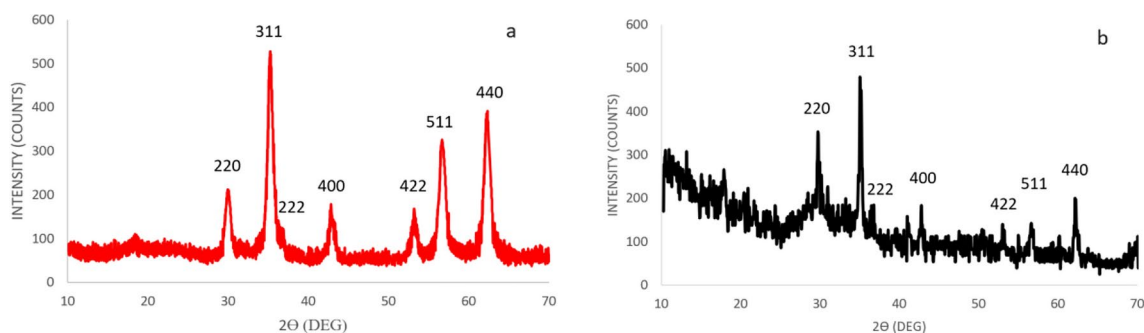


Fig. 3. XRD spectrum of (a) AlFe_2O_4 and (b) $\text{AlFe}_2\text{O}_4@n\text{-Pr}@Et\text{-SO}_3\text{H}$.

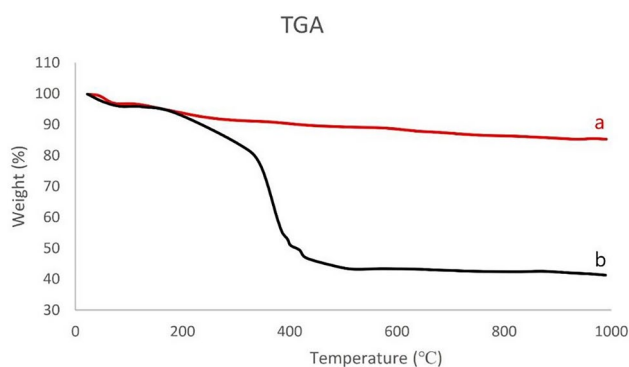


Fig. 4. TGA curve of (a) AlFe_2O_4 , (b) $\text{AlFe}_2\text{O}_4@n\text{-Pr}@Et\text{-SO}_3\text{H}$.

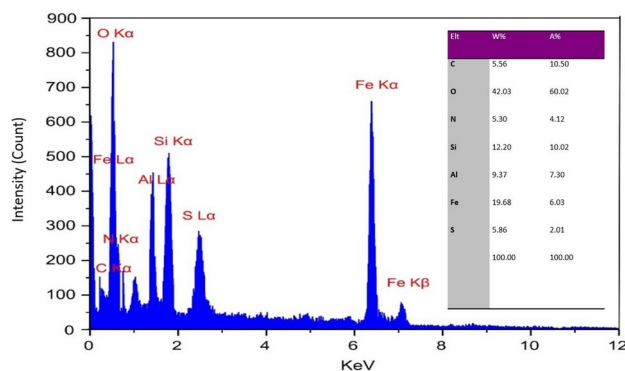


Fig. 5. EDX images of $\text{AlFe}_2\text{O}_4@n\text{-Pr}@Et\text{-SO}_3\text{H}$.

in peak intensity was observed for $\text{AlFe}_2\text{O}_4@n\text{-Pr}@Et\text{-SO}_3\text{H}$, along with increased background noise. These observations suggest that the textural characteristics of AlFe_2O_4 were maintained during the preparation of the SO_3H -supported catalyst, with its crystalline phase and structural properties remaining intact^{36–38}.

An investigation using TGA was conducted to quantitatively assess the presence of the ligand ($\text{Et-SO}_3\text{H}$) on the surface of AlFe_2O_4 magnetic nanoparticles. Weight loss below 250 °C is linked to the removal of organic solvents (Fig. 4a). Specifically, 15% of the weight loss in this temperature range is due to organic solvents (Fig. 4b). In Fig. 4b, it is noted that $\text{AlFe}_2\text{O}_4@n\text{-Pr}@Et\text{-SO}_3\text{H}$ shows a 35% weight reduction between 250 and 600 °C, indicating the decomposition of its constituents. The TGA analysis thus confirmed the successful anchoring of $-\text{SO}_3\text{H}$ groups on the surface of AlFe_2O_4 MNPs.

To gain insight into the chemical composition of the nanocomposite, an energy-dispersive X-ray (EDX) analysis was conducted. Figure 5 illustrates the profile, depicting Fe and Al as the metallic components. The successful formation of a sulfuric acid shell on the surface of AlFe_2O_4 has been confirmed by the presence of sulfur and oxygen. Furthermore, the absence of any other elements indicates the high purity of the sample. The sulfur presence was indeed detected, but no amount of Cl was observed, indicating that the covalent adsorption of SO_3H groups had successfully taken place on the catalyst surface.

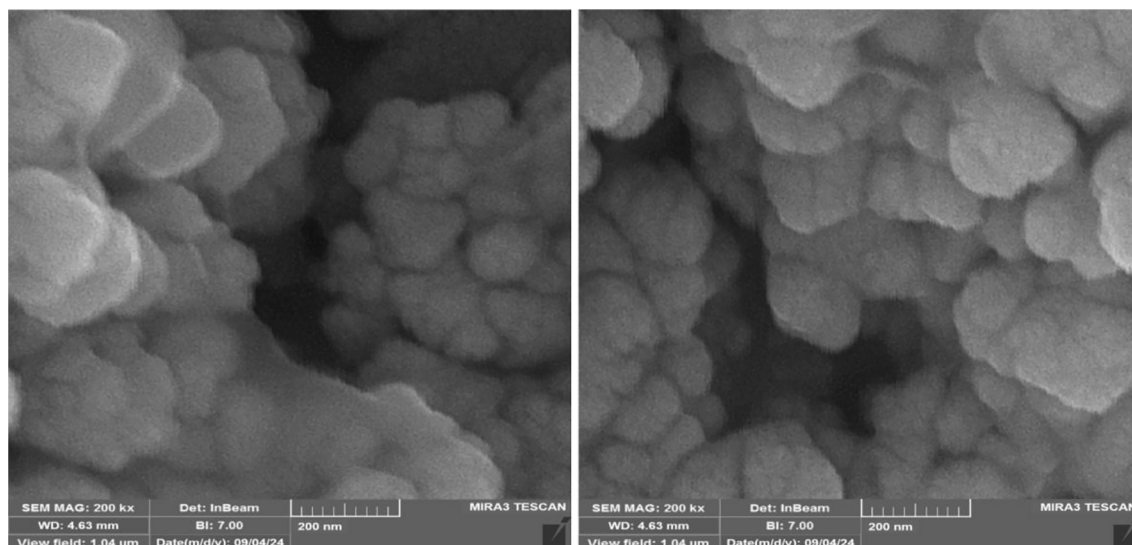


Fig. 6. SEM images of $\text{AlFe}_2\text{O}_4@n\text{-Pr}@Et\text{-SO}_3\text{H}$.

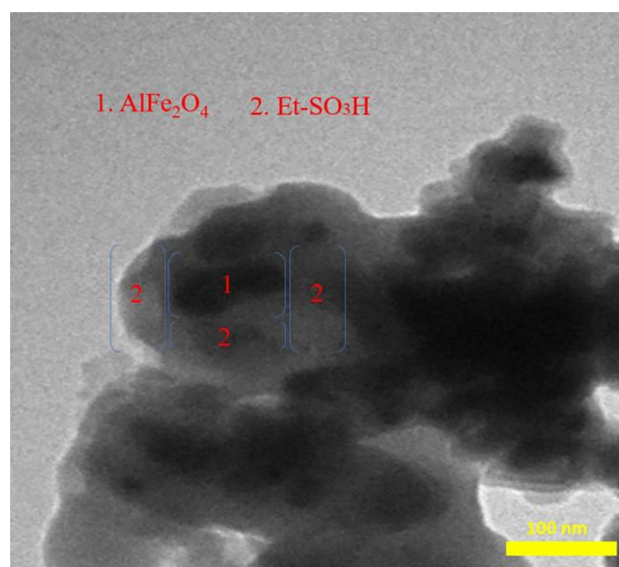


Fig. 7. TEM images of $\text{AlFe}_2\text{O}_4@n\text{-Pr}@Et\text{-SO}_3\text{H}$.

Figure 6 presents the SEM analysis of $\text{AlFe}_2\text{O}_4@n\text{-Pr}@Et\text{-SO}_3\text{H}$, illustrating its morphology and dimensions. This analysis clearly reveals the uniform spherical shape of the nanocomposite, featuring a rough surface texture. Importantly, no significant aggregation was observed in the sample, suggesting a successful distribution and stability of the nanocomposite.

Transmission electron microscopy (TEM) was used to evaluate the shape, size, and morphology of $\text{AlFe}_2\text{O}_4@n\text{-Pr}@Et\text{-SO}_3\text{H}$ magnetic nanoparticles (MNPs). Figure 7 depicts TEM images showing spherical ferrite materials with smooth surfaces at various magnifications. The image distinguishes between the darker layer, which represents the AlFe_2O_4 substrate, and the lighter layer, identifying the $\text{Et-SO}_3\text{H}$ attached to the substrate. These materials exhibit a uniform, amorphous phase of $\text{Et-SO}_3\text{H}$ that is evenly distributed on the surface of a typical AlFe_2O_4 spinel core. The presence of a light shell over the core further supports the hypothesis that SO_3H functionalities, along with Et moieties, are immobilized on its surface (Fig. 7).

The magnetic properties and values of the nanocomposites AlFe_2O_4 , $\text{AlFe}_2\text{O}_4@n\text{-Pr}$, and $\text{AlFe}_2\text{O}_4@n\text{-Pr}@Et\text{-SO}_3\text{H}$ were additionally assessed through VSM measurements at room temperature (Fig. 8). The saturation magnetization (M_s) values for (a) AlFe_2O_4 , (b) $\text{AlFe}_2\text{O}_4@n\text{-Pr}$, and (c) $\text{AlFe}_2\text{O}_4@n\text{-Pr}@Et\text{-SO}_3\text{H}$ are 68, 49, and 27 emu g^{-1} , respectively. The values make it clear that the magnetization value of the samples was significantly reduced through surface modification and catalytic functional group immobilization on the AlFe_2O_4 support. However, the MNPs targeted displayed outstanding superparamagnetic properties and can be easily separated.

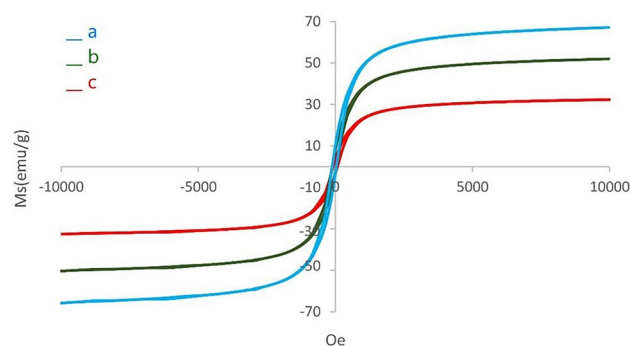


Fig. 8. VSM curves of (a) AlFe_2O_4 , (b) $\text{AlFe}_2\text{O}_4@n\text{-Pr}$ (c) $\text{AlFe}_2\text{O}_4@n\text{-Pr}@Et\text{-SO}_3\text{H}$.

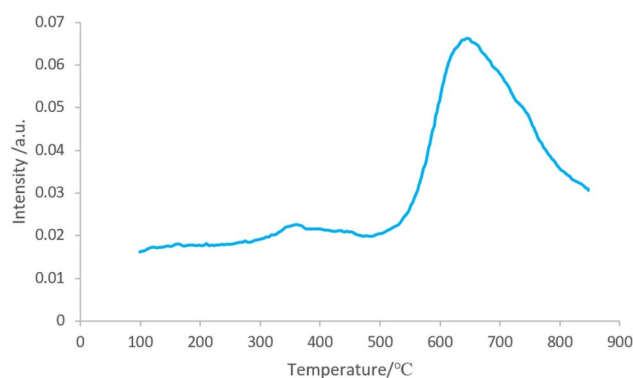


Fig. 9. The NH_3 -TPD of $\text{AlFe}_2\text{O}_4@n\text{-Pr}@Et\text{-SO}_3\text{H}$.

NH₃-TPD results

To examine the acidity of the $\text{AlFe}_2\text{O}_4@n\text{-Pr}@Et\text{-SO}_3\text{H}$ catalysts, NH_3 -TPD analysis was conducted, and the findings are presented in Fig. 9. Typically, ammonia desorption from alumina-based catalysts occurs within the 100–900 °C temperature range. The TPD profile for the $\text{AlFe}_2\text{O}_4@n\text{-Pr}@Et\text{-SO}_3\text{H}$ catalyst revealed two distinct ammonia desorption peaks. The first peak at 350 °C indicates desorption from sites with moderate acidity, while the high-temperature peak at 630 °C reflects desorption from strong acidic sites. Figure 9 shows clearly the $\text{AlFe}_2\text{O}_4@n\text{-Pr}@Et\text{-SO}_3\text{H}$ sample possess both weak and strong acid sites.

Catalytic studies

Esterification reactions

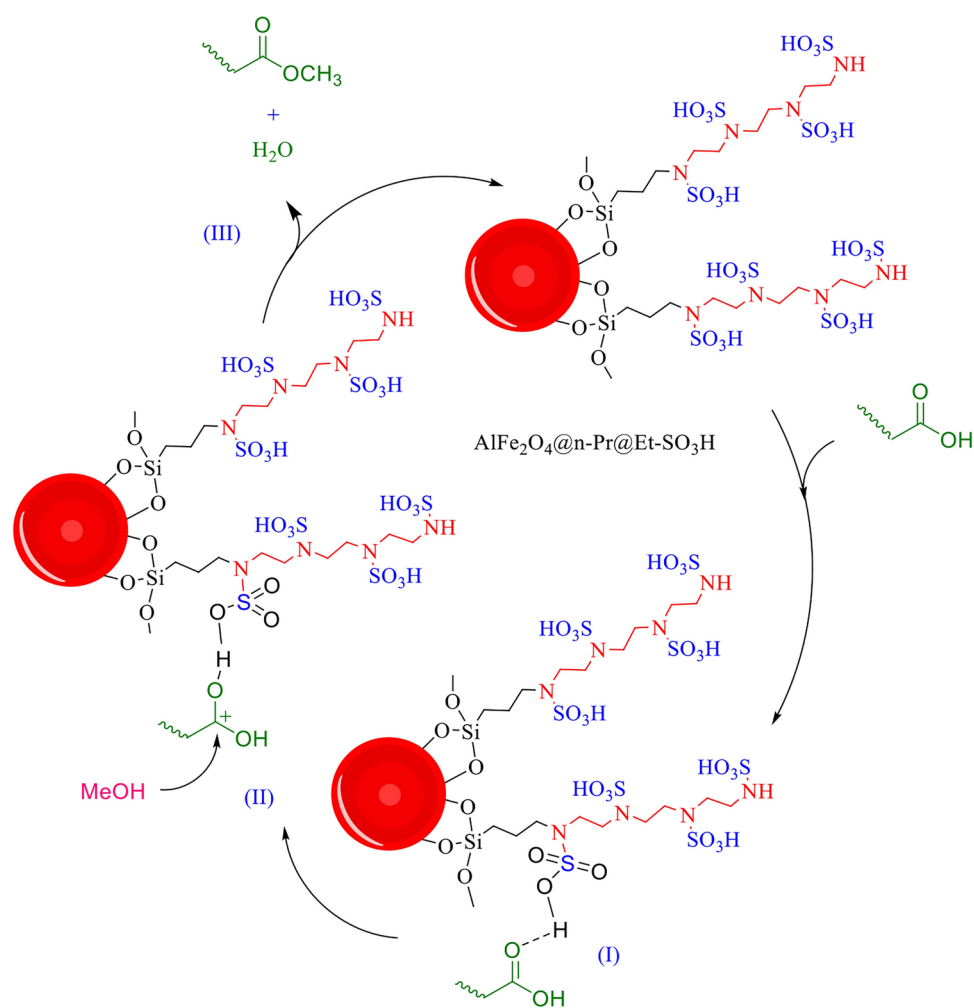
The catalytic activity of $\text{AlFe}_2\text{O}_4@n\text{-Pr}@Et\text{-SO}_3\text{H}$ was evaluated during the esterification of oleic acid with methanol, as detailed in Table 1. To determine the optimal conditions for biodiesel production using this catalyst, the study explored various parameters, including temperature, the molar ratio of methanol to oleic acid, and the amount of catalyst used. Repeated reactions with varying amounts of $\text{AlFe}_2\text{O}_4@n\text{-Pr}@Et\text{-SO}_3\text{H}$ under consistent conditions showed a significant yield increase, up to 98%, when employing 0.04 g of the catalyst (see Table 1, entries 2–5). The influence of different temperatures on the reaction was also assessed (Table 1, entries 6 and 7), identifying 60 °C as the most effective for product formation. These observations led to the conclusion that the highest biodiesel yield was achieved with 0.04 g of the nanocatalyst at 60 °C, achieving a conversion rate of 98% from oleic acid to ester. The study highlighted a 3:12 molar ratio between oleic acid and methanol as being vital for successful esterification (see Table 1, entries 8–11). Typically, an excess of alcohol helps to disperse the solid acid catalyst in oily media and enhances the interaction between reactants, thereby boosting biodiesel yield. Furthermore, as is common in esterification processes, an excess of alcohol can prevent the reverse reaction, contributing to a gradual increase in ester production over time.

The mechanism of the $\text{AlFe}_2\text{O}_4@n\text{-Pr}@Et\text{-SO}_3\text{H}$ catalytic esterification is illustrated in Scheme 4 and can be broken down into three stages. Initially, $\text{AlFe}_2\text{O}_4@n\text{-Pr}@Et\text{-SO}_3\text{H}$ acts as a catalyst by activating the carbonyl group of oleic acid, leading to the formation of positive carbon ions. Subsequently, methanol molecules interact with these positive carbon ions to create intermediate products. This is followed by the transfer of hydrogen ions from intermediate product II, resulting in the formation of a protonated hydroxyl group. During this process, water molecules are eliminated from the main chain of product II. Ultimately, methyl oleate is formed as product III, and the heterogeneous catalyst $\text{AlFe}_2\text{O}_4@n\text{-Pr}@Et\text{-SO}_3\text{H}$ is then separated from the final mixture^{3,39}.

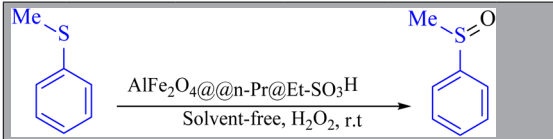
To improve the reaction conditions, we studied the oxidation process of methyl phenyl sulfide as a model compound using H_2O_2 under various reaction parameters, such as time and product yield (refer to Table 2).

Entry ^a	Catalyst amount (g)	Temperature (°C)	Methanol/oleic acid molar ratio (mmol/mmol)	Time (h)	Biodiesel produced (mg)	Unreacted material (mg)	Biodiesel yield (%)
1	–	60	12:3	12	–	–	N. R
2	0.02	60	12:2	2	0.093	0.42	40
3	0.03	60	12:3	2	0.139	0.63	60
4	0.04	60	12:3	2	0.227	0.01	98
5	0.05	60	12:3	2	0.183	0.82	79
6	0.04	25	12:3	2	0.111	0.50	48
7	0.04	50	12:3	2	0.139	0.63	60
8	0.04	60	9:3	2	0.153	0.69	66
9	0.04	60	8:3	2	0.116	0.52	50
10	0.04	60	11:3	2	0.146	0.66	63
11	0.04	60	15:3	2	0.167	0.75	72

Table 1. Material balance calculations for the optimized yield of biodiesel in the presence of $\text{AlFe}_2\text{O}_4@n\text{-Pr}@Et\text{-SO}_3\text{H}$.



Scheme 4. Proposed Mechanism for biodiesel in this presence of $\text{AlFe}_2\text{O}_4@n\text{-Pr}@Et\text{-SO}_3\text{H}$.



Entry	Catalyst (g)	Solvent	H ₂ O ₂ (mg)	Time (min)	Yield
1	–	Solvent-free	0.4	5 h	Trace
2	0.005	Solvent-free	0.4	30	45
3	0.01	Solvent-free	0.4	30	81
4	0.02	Solvent-free	0.4	30	99
5	0.03	Solvent-free	0.4	30	99
6	0.02	PEG	0.4	30	57
7	0.02	H ₂ O: EtOH	0.4	30	46
8	0.02	DMSO	0.4	30	49
9	0.02	EtOH	0.4	30	78
10	0.02	Solvent-free	0.3	30	90
11	0.02	Solvent-free	0.5	30	97

Table 2. Optimizing reaction conditions for oxidation of methyl phenyl sulfide in the presence of $\text{AlFe}_2\text{O}_4@n\text{-Pr@Et-SO}_3\text{H}$.

According to the table, the reaction remained incomplete without $\text{AlFe}_2\text{O}_4@n\text{-Pr@Et-SO}_3\text{H}$ even after 5 h. When a catalytic amount of $\text{AlFe}_2\text{O}_4@n\text{-Pr@Et-SO}_3\text{H}$ (0.02 g) was used under solvent-free conditions at room temperature, H_2O_2 was identified as the most effective reagent for achieving complete conversion of methyl phenyl sulfide to methyl phenyl sulfoxide.

The versatility of this method has been proven by the easy conversion of aryl, cyclic, benzylic, and linear sulfides, as depicted in Table 3. The sulfoxides were rapidly obtained with excellent yields. To showcase the chemical selectivity of the process, sulfides containing oxidation-prone and acid-sensitive functional groups such as CHO, OH, and CO_2CH_3 were employed in the sulfoxidation reaction. Importantly, these functional groups remained unaltered during the conversion from sulfide to sulfoxide, as illustrated in Table 3.

Scheme 5 outlines a potential pathway for the oxidation of sulfides. One approach involves the in-situ formation of peroxy acid when $\text{AlFe}_2\text{O}_4@n\text{-Pr@Et-SO}_3\text{H}$ reacts with H_2O_2 , subsequently transferring oxygen to the organic substrate (illustrated in Scheme 5a). Alternatively, another approach suggests that $\text{AlFe}_2\text{O}_4@n\text{-Pr@Et-SO}_3\text{H}$ acts as a protic acid, polarizing the O–O bond in hydrogen peroxide to produce the reactive oxygen transfer agent (depicted in Scheme 5b).

Hot filtration

To demonstrate heterogeneity, two parallel reactions were conducted under identical conditions using oleic acid and methanol for esterification in the presence of a catalyst at 65 °C in ethanol. After 60 min, one reaction was halted, achieving a yield of 47%. Simultaneously, the catalyst was removed from the second reaction, allowing it to proceed without the catalyst for an additional 60 min, resulting in a 51% yield. The minor 4% increase in conversion underscores the role and heterogeneity of the catalyst.

Catalyst recyclability

To further investigate the recyclability of the magnetic nanocatalyst, we conducted a reaction between oleic acid and methanol using 0.04 g of $\text{AlFe}_2\text{O}_4@n\text{-Pr@Et-SO}_3\text{H}$ as our model. The nanocatalyst was separated from the reaction mixture with a magnet and washed several times with water and ethanol. It was reused for over five cycles without any significant loss of activity, as shown in Fig. 10. Thanks to its excellent recovery from the reaction mixture, together with its stability and resistance to decomposition, the catalyst can be retrieved and reused multiple times. It maintained its activity over five consecutive cycles, highlighting its robustness.

In Table 4, the catalytic activities of previously documented solid acid catalysts are contrasted with those of our prepared $\text{AlFe}_2\text{O}_4@n\text{-Pr@Et-SO}_3\text{H}$ in the esterification of oleic acid with methanol. Solid acid catalysts show better catalytic efficiency in less time compared to $\text{AlFe}_2\text{O}_4@n\text{-Pr@Et-SO}_3\text{H}$ catalyst under the given reaction conditions. This shows that the $\text{AlFe}_2\text{O}_4@n\text{-Pr@Et-SO}_3\text{H}$ catalyst is more effective in esterification reactions than previous ones (refer to Table 4).

Conclusion

This study outlines the development of an efficient method for producing $\text{AlFe}_2\text{O}_4@n\text{-Pr@Et-SO}_3\text{H}$, an innovative and eco-friendly magnetic nanocatalyst that is easy to recover. The catalyst was characterized using techniques like EDS, SEM, VSM, XRD, TGA, TEM, and FT-IR. It was applied in esterification reactions and the oxidation of sulfides. The synthesis of this nanocatalyst involves readily available materials and features a simplified work-up procedure. Advantages of this method include the use of a non-toxic solvent, high yield, short reaction time, compatibility with various functional groups, and the ability to recycle and reuse the catalyst with an external magnet for up to four cycles with minimal reduction in product yields.

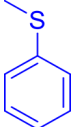
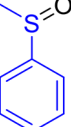
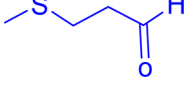
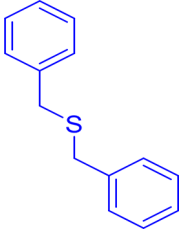
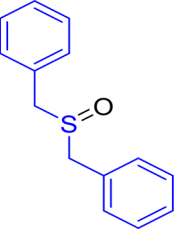
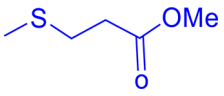
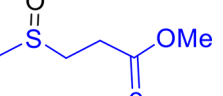
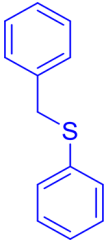
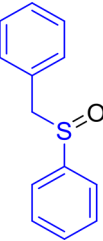
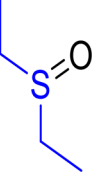
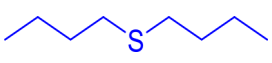
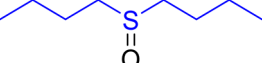
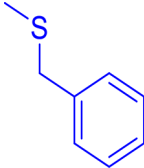
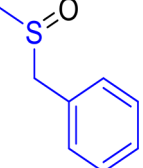
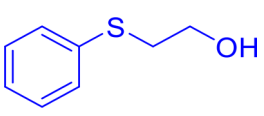
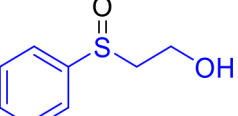
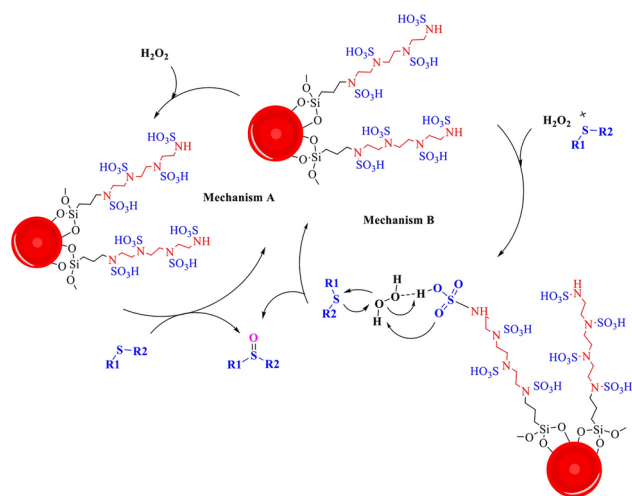
Entry	Substrate	Product	Time(min)	Yield (%)
1			30	99
2			45	90
3			20	94
4			60	93
5			15	95
6			60	95
7			60	86
8			20	91
9			20	92

Table 3. Oxidation of sulfides into sulfoxides in the presence of $\text{AlFe}_2\text{O}_4@n\text{-Pr@Et-SO}_3\text{H}$.



Scheme 5. The suggested mechanism for the oxidation of sulfide.

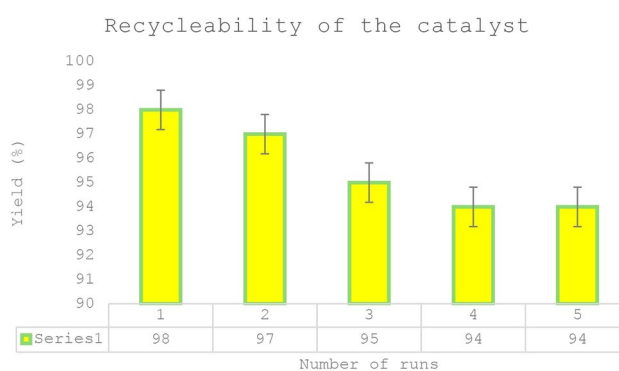


Fig. 10. Recyclability of $\text{AlFe}_2\text{O}_4@n\text{-Pr}@Et\text{-SO}_3\text{H}$.

Entry	Cat	Molar ratio	T (°C)	Time (h)	Yield (%)	References
1	HZSM-5	1:45	130	7	80	40
2	1S/ZSM-5	1:20	190	8	97	41
3	Citric acid/HZSM-5	1:45	100	4	83	42
4	$\text{AlFe}_2\text{O}_4@n\text{-Pr}@Et\text{-SO}_3\text{H}$	12:3	60	2	98	This work

Table 4. Comparison of the catalytic efficiency of reported acid catalysts with prepared $\text{AlFe}_2\text{O}_4@n\text{-Pr}@Et\text{-SO}_3\text{H}$ catalyst in the esterification of oleic acid with methanol.

Data availability

All data generated or analyzed during this study are included in this published article [and its supplementary information files].

Received: 5 September 2024; Accepted: 24 December 2024

Published online: 09 January 2025

References

- Chehab, S., Merroun, Y., Ghailane, R., Boukhris, S. & Souizi, A. $\text{Na}_2\text{Ca}(\text{HPO}_4)_2$, an efficient, reusable eco-friendly catalyst for the synthesis of 1,8-dioxo-octahydroxanthenes and biscoumarin derivatives. *Polycyclic Aromat. Compd.* **43**, 4906–4923 (2023).
- Chutia, G. P. & Phukan, K. Facile synthesis of $\text{Fe}_3\text{O}_4@biochar@SO_3\text{H}$ as magnetically separable Bronsted acid nanocatalyst for biodiesel production from different oil feedstocks. *Ind. Crops Prod.* **215**, 118578 (2024).
- Zhang, Q. et al. Efficient biodiesel production from oleic acid using metal-organic framework encapsulated Zr-doped polyoxometalate nano-hybrids. *RSC Adv.* **10**, 8766–8772 (2020).
- Rangraz, Y., Nemat, F. & Elhampour, A. A novel magnetically recoverable palladium nanocatalyst containing organoselenium ligand for the synthesis of biaryls via Suzuki-Miyaura coupling reaction. *J. Phys. Chem. Solids* **138**, 109251 (2020).

5. Zhao, H. et al. In vitro toxicity evaluation of ultra-small MFe_2O_4 ($M = Fe, Mn, Co$) nanoparticles using A549 cells. *RSC Adv.* **5**, 68454–68460 (2015).
6. Singh, C., Devika, D., Malik, R., Kumar, V. & Singhal, S. CdS nanorod- MFe_2O_4 ($M = Zn, Co$ and Ni) nanocomposites: A heterojunction synthesis strategy to mitigate environmental deterioration. *RSC Adv.* **5**, 89327–89337 (2015).
7. Zhang, M. et al. Synthesis, characterization and catalytic behavior of MFe_2O_4 ($M = Ni, Zn$ and Co) nanoparticles on the thermal decomposition of TKX-50. *J. Therm. Anal. Calorim.* **141**, 1413–1423 (2020).
8. Vibhute, S. P., Mhaldar, P. M., Shejwal, R. V. & Pore, D. M. Magnetic nanoparticles-supported palladium catalyzed Suzuki-Miyaura cross coupling. *Tetrahedron Lett.* **61**, 151594 (2020).
9. Pormazar, S. M. & Dalvand, A. Adsorption of Reactive Black 5 azo dye from aqueous solution by using amine-functionalized Fe_3O_4 nanoparticles with L-arginine: Process optimisation using RSM. *Int. J. Environ. Anal. Chem.* **00**, 1–20 (2020).
10. Zhu, Z., Zhang, W. & Gao, Z. Suzuki-Miyaura carbonylative reaction in the synthesis of biaryl ketones. *Progress Chem.istry* **28**, 1626–1633 (2016).
11. Han, J. S. & An, G. S. Preparation of dual-layered core-shell $Fe_3O_4@SiO_2$ nanoparticles and their properties of plasmid DNA purification. *Nanomaterials* **11**, 3422 (2021).
12. Liao, J. et al. 3D core-shell $Fe_3O_4@SiO_2@MoS_2$ composites with enhanced microwave absorption performance. *J. Colloid Interface Sci.* **604**, 537–549 (2021).
13. Sathish, T. et al. Enhanced waste cooking oil biodiesel with Al_2O_3 and MWCNT for CI engines. *Fuel* **333**, 126429 (2023).
14. Banerjee, B. et al. Sodium dodecyl sulphate catalyzed one-pot three-component synthesis of structurally diverse 2-amino-3-cyano substituted Tetrahydrobenzo[b]pyrans and spiropyran in water at room temperature. *Catal. Lett.* <https://doi.org/10.1007/s10562-022-04256-0> (2023).
15. Nguyen, N. T. T., Nguyen, T. T. T., Nguyen, D. T. C. & Tran, T. V. Green synthesis of $ZnFe_2O_4$ nanoparticles using plant extracts and their applications: A review. *Sci. Total Environ.* **872**, 162212 (2023).
16. Anizadeh, M. R., Torabi, M., Zolfigol, M. A. & Yarie, M. Catalytic application $Fe_3O_4@SiO_2@(CH_2)_3$ -urea-dithiocarbamic acid for the synthesis of triazole-linked pyridone derivatives. *J. Mol. Struct.* **1277**, 134885 (2023).
17. Zhang, X. et al. Effect of benzoic acid and dopamine hydrochloride as a modulator in the water resistance of Universitetet i Oslo-67: Adsorption performance and mechanism. *J. Colloid Interface Sci.* **651**, 424–435 (2023).
18. Taheri-Ledari, R. et al. Facile route to synthesize $Fe_3O_4@acacia-SO_3H$ nanocomposite as a heterogeneous magnetic system for catalytic applications. *RSC Adv.* **10**, 40055–40067 (2020).
19. Elsayed, I., Mashaly, M., Eltaweel, F., Jackson, M. A. & Hassan, E. B. Dehydration of glucose to 5-hydroxymethylfurfural by a core-shell $Fe_3O_4@SiO_2-SO_3H$ magnetic nanoparticle catalyst. *Fuel* **221**, 407–416 (2018).
20. Wang, C. et al. Photothermal suzuki coupling over a metal halide perovskite/Pd nanocube composite catalyst. *ACS Appl. Mater. Interfaces* **14**, 17185–17194 (2022).
21. Nigam, A. & Pawar, S. J. Structural, magnetic, and antimicrobial properties of zinc doped magnesium ferrite for drug delivery applications. *Ceram. Int.* **46**, 4058–4064 (2020).
22. Patil, P. et al. [MerDABCO- SO_3H]Cl catalyzed synthesis, antimicrobial and antioxidant evaluation and molecular docking study of pyrazolopyranopyrimidines. *J. Mol. Struct.* **1242**, 130672 (2021).
23. Ferreira, A. B., Lemos Cardoso, A. & da Silva, M. J. Tin-catalyzed esterification and transesterification reactions: A review. *ISRN Renew. Energy* **2012**, 142857 (2012).
24. Mandari, V. & Devarai, S. K. Biodiesel production using homogeneous, heterogeneous, and enzyme catalysts via transesterification and esterification reactions: A critical review. *Bioenergy Res.* **15**, 935–961 (2022).
25. Khan, Z. et al. Current developments in esterification reaction: A review on process and parameters. *J. Ind. Eng. Chem.* **103**, 80–101 (2021).
26. Moradi, P., Saidi, M. & Najafabadi, A. T. Biodiesel production via esterification of oleic acid as a representative of free fatty acid using electrolysis technique as a novel approach: Non-catalytic and catalytic conversion. *Process Safety Environ. Protect.* **147**, 684–692 (2021).
27. Prabhu, C. et al. Biodiesel unsaturation and the synergic effects of hydrogen sharing rate on the characteristics of a compression ignition engine in dual-fuel mode. *Fuel* **334**, 126699 (2023).
28. Ye, C., Qi, Z., Cai, D. & Qiu, T. Design and synthesis of ionic liquid supported hierarchically porous Zr Metal-organic framework as a novel Brønsted–Lewis acidic catalyst in biodiesel synthesis. *Ind. Eng. Chem. Res.* **58**, 1123–1132 (2019).
29. Lin, C.-H., Chang, Y.-T., Lai, M.-C., Chiou, T.-Y. & Liao, C.-S. Continuous biodiesel production from waste soybean oil using a nano- Fe_3O_4 microwave catalysis. *Processes* **9**, 756 (2021).
30. Stegarescu, A. et al. Nanocomposite based on Fe_3O_4/MnO_2 for biodiesel production improving. *Chem. Papers* **75**, 3513–3520 (2021).
31. Guo, M. et al. Process optimization of biodiesel production from waste cooking oil by esterification of free fatty acids using $La^{3+}/ZnO-TiO_2$ photocatalyst. *Energy Convers. Manag.* **229**, 113745 (2021).
32. Wang, L., Zhang, Y., Yao, J. & Li, H. Metal-free synthesis of sulfones and sulfoxides through aldehyde-promoted aerobic oxidation of sulfides. *Catal. Lett.* <https://doi.org/10.1007/s10562-021-03706-5> (2021).
33. Elgorban, A. M., Marraiki, N., Ansari, S. A. & Syed, A. Green synthesis of Cu/Fe_3O_4 nanocomposite using Calendula extract and evaluation of its catalytic activity for chemoselective oxidation of sulfides to sulfoxides with aqueous hydrogen peroxide. *J. Organomet. Chem.* **954–955**, 122077 (2021).
34. Ahmad, I. & Dhar, R. Sulfonic acid-functionalized solid acid catalyst in esterification and transesterification reactions. *Catal. Surv. Asia* **21**, 53 (2017).
35. Devasan, R. et al. Microwave-assisted biodiesel production using bio-waste catalyst and process optimization using response surface methodology and kinetic study. *Sci. Rep.* **2570**, <https://doi.org/10.1038/s41598-023-29883-4> (2023).
36. Silva, J. M., Araújo, J. F. D. F., Brocchi, E. & Solórzano, I. G. Micro analytical and magnetic characterization of aluminum-iron spinel ($FeAl_2O_4$) synthesized by combustion reaction. *Ceram. Int.* **46**, 19052–19061 (2020).
37. Dong, Y. et al. Mechanical characteristics of $FeAl_2O_4$ and $AlFe_2O_4$ spinel phases in coatings—A study combining experimental evaluation and first-principles calculations. *Ceram. Int.* **43**, 16094–16100 (2017).
38. Verwey, E. J., Haayman, P. W. & Romeijn, F. C. Physical properties and cation arrangement of oxides with spinel structures II. Electronic conductivity. *J. Chem. Phys.* **15**, 181–187 (1947).
39. Bian, Y., Shan, Q., Guo, C., Liu, C. & Zhang, J. Biodiesel production over esterification catalyzed by a novel poly(acidic ionic liquid)s. *Catal. Lett.* **151**, 3523–3531 (2021).
40. Vieira, S. S. et al. Biodiesel production by free fatty acid esterification using lanthanum (La^{3+}) and HZSM-5 based catalysts. *Bioresour. Technol.* **133**, 248–255 (2013).
41. Mohebbi, S., Rostamizadeh, M. & Kahroushan, D. Efficient sulfated high silica ZSM-5 nanocatalyst for esterification of oleic acid with methanol. *Microporous Mesoporous Mater.* **294**, 109845 (2020).
42. Vieira, S. S. et al. Use of HZSM-5 modified with citric acid as acid heterogeneous catalyst for biodiesel production via esterification of oleic acid. *Microporous Mesoporous Mater.* **201**, 160–168 (2015).

Acknowledgements

The authors present their appreciation to King Saud University for funding this research through Researchers Supporting Program number (RSPD2025R779), King Saud University, Riyadh, Saudi Arabia

Author contributions

D.S., K.S., Y.J., S.V.M., P.S., S.M.I., and M.S., Funding acquisition, Supervision, Conceptualization, Resources, Writing-review & editing. M.K.A., S.B.A.R., and M.A.E.-M., Methodology, Writing—original draft.

Declarations

Competing interests

The authors declare no competing interests.

Additional information

Correspondence and requests for materials should be addressed to D.S.

Reprints and permissions information is available at www.nature.com/reprints.

Publisher's note Springer Nature remains neutral with regard to jurisdictional claims in published maps and institutional affiliations.

Open Access This article is licensed under a Creative Commons Attribution-NonCommercial-NoDerivatives 4.0 International License, which permits any non-commercial use, sharing, distribution and reproduction in any medium or format, as long as you give appropriate credit to the original author(s) and the source, provide a link to the Creative Commons licence, and indicate if you modified the licensed material. You do not have permission under this licence to share adapted material derived from this article or parts of it. The images or other third party material in this article are included in the article's Creative Commons licence, unless indicated otherwise in a credit line to the material. If material is not included in the article's Creative Commons licence and your intended use is not permitted by statutory regulation or exceeds the permitted use, you will need to obtain permission directly from the copyright holder. To view a copy of this licence, visit <http://creativecommons.org/licenses/by-nc-nd/4.0/>.

© The Author(s) 2025